EFFECTS OF SECONDARY ELECTRON EMISSION ON CHARGING*

Martin S. Leung, Michael B. Tueling, and Edwin R. Schnauss
The Aerospace Corporation

ABSTRACT

A detailed description of the secondary electron emission characteristics is essential to the understanding of the charging behaviors of various dielectrics. Laboratory charging studies using two electron sources with different energies show that the charging behaviors of typical spacecraft thermal control dielectric surfaces are extremely sensitive to the shape of their secondary emission curves. The results also suggest that the electron spectrum in a natural charging environment can be separated into three distinct regions (noninteracting, discharging, and charging) depending on the kinetic energy of the incident electron relative to the charged surface, and on the secondary emission characteristics of the material. To a first order approximation, the relative number of electrons in these different regions determines the potential of the charged surface. In this paper, we report detailed measurements of the secondary electron emission characteristics of Kapton, and also discuss the effects of bulk conductivity and secondary emission on surface charging of these materials.

INTRODUCTION

The understanding of material charging requires a detailed knowledge of both the charging environment (ref. 1) and certain electronic properties of the material (ref. 2). Under electron irradiation and in the absence of photoillumination, the equilibrium surface potential is determined by two basic material properties: its conductivity, and secondary electron emission. The relative importance of these two properties depends on the magnitude of the incident current compared to the bulk leakage current. In conductors and semiconductors, the leakage current is high and the material behaves as a simple ohmic element, i.e., the surface voltage is directly proportional to the incident current density. In the case of low-conductivity materials, the incoming current is not necessarily dissipated by the leakage current, resulting in a charge buildup in the material. Such a buildup retards the incident current and modifies the kinetic energy of the electrons such that there is an increase in the number of secondary electrons emitted from the surface. Eventually, the surface will charge to an equilibrium potential, at which point, the incoming primaries will be balanced by the outgoing secondaries. In this limit, the equilibrium surface potential is controlled by the secondary electron emission behavior of the target material. The purpose of this paper is to discuss the effects of secondary emission on material charging under single and dual energy electron irradiation, and to present novel techniques for measuring secondary emission parameters in the laboratory. We would also like to

*This work was supported by the U.S. Air Force Space Division under Contract F04701-80-C-0081.

point out how these parameters can be used to add to the understanding of material charging in an environment where the electrons are distributed both in energy and space.

BACKGROUND

When a solid is bombarded with energetic electrons in the keV range, a large number of low energy secondary electrons are generated in the solid within a certain distance from the surface. The secondaries which have the appropriate trajectories and sufficient energy to overcome the work function of the surface can escape from the solid. A number of authors (ref. 3) have written on the theoretical as well as the experimental aspects of the basic phenomenon. In general, it is found that the number of secondary electrons emitted depends critically on the kinetic energy of the primary electrons. In addition, it is also observed that the yield curve describing the production of the secondaries as a function of the primary electron energy can be reduced to fit a universal shape. A "typical" secondary yield curve for an insulator is shown in figure 1. The curve is a plot of δ, the number of secondaries emitted per incident primary, as a function of the kinetic energy of the primary electrons at the surface. At low incident kinetic energy, the electrons striking the surface do not have sufficient energy to generate large numbers of secondaries and hence δ is less than unity. As the kinetic energy increases, although the incident electrons penetrate deeper into the material, more secondaries are being created and allowed to escape giving rise to a δ which can be significantly greater than unity. Thus, δ will continue to increase rapidly until the penetration depth most favorable for the production of secondaries is reached. At this point, δ reaches a maximum (δ_{max}) at energy E_{max}. Beyond this point, the number of electrons emitted decreases because the bulk of the internal secondaries are generated increasingly deeper in the solid reducing the probability of escape. This results in $\delta < 1$ at high incident electron energies. Depending on the material and its structure, the values of δ_{max} and E_{max} can differ widely. For most insulating materials, such as metal oxides and organic polymers, δ_{max} is usually greater than unity. In these materials, two other energies in the secondary yield curve are important for describing material charging. They are the first and second crossover points, E_I and E_{II}, where $\delta = 1$. In particular, E_{II} is especially important to material charging due to electron bombardment.

In terms of theoretical treatment of secondary emission, the formulation given by Sternglass (ref. 4) has been found to be in fairly close agreement with experimental measurements. This formulation assumes that all the secondary electrons are generated at a mean depth, λ_m, where the average forward momentum of the primaries vanishes. Secondly, the model assumes that the fraction of the secondaries escaping from the surface decreases exponentially with the depth of generation. Further considerations show that λ_m is proportional to the square root of the primary energy, E. Therefore, the fraction of secondary electrons emitted is proportional to $\exp(-\beta E^{1/2})$, where β is a constant related to the escape depth of the material. The total secondary yield is then given by

$$\delta(E) = AE \cdot \exp(-\beta E^{1/2}) \qquad (1)$$

where A is material dependent parameter, characteristic of the efficiency of secondary electron emission and backscattering. For a particular material, $\delta(E)$ is fixed by two points, $\delta(E_{II}) = 1$ and

$$\left.\frac{d\delta(E)}{dE}\right|_{E_{max}} = 0$$

Hence, equations (1) can be rewritten as

$$\delta(E) = \frac{E}{E_{II}} \cdot \exp\left[-\frac{2}{E_{max}^{1/2}}\left(E^{1/2} - E_{II}^{1/2}\right)\right] \qquad (2)$$

E_{max} and E_{II} in equation (2) control the shape of the secondary yield curve. In the following, we shall describe how these parameters are determined in the laboratory and how they can affect material charging in space.

EXPERIMENT

Our technique to study secondary emission was based on measuring the back surface electric field of a sample film while the front surface was irradiated with either one or two monoenergetic electron beams. The back field measurement method was the same as the one used in the Satellite Surface Potential Monitor (SSPM) for determining material charging aboard the P78-2 SCATHA satellite (ref.5). The crucial part of the instrument consists of an electrostatic field meter placed at a fixed distance behind the dielectric film sample which was mounted rigidly on a holder with conductive epoxy. The samples used in the measurement were common external spacecraft thermal control surfaces, in many cases they were polymers with their back surfaces metalized. Therefore, a small portion of the metalization had to be removed to enable the electric field due to the charge build-up to terminate at the sensor. The removal of metalization lowers the capacitance of the film in the region where the measurement is made, causing that portion of the film to charge much more rapidly than the rest of the sample. However, at equilibrium, independent measurement of the front surface potential profile showed that the potentials of the metalized and the unmetalized portions of the film are equal. Moreover, the back and the front surface measurements were sufficiently well correlated that the back surface field can be calibrated to infer the front surface potential accurately. In addition, the back metalization acts as a collector for the current passing through the bulk of the film. Hence, this configuration provides the measurement of both the surface potential as well as the leakage current at equilibrium simultaneously.

In the laboratory, the front surface of the sample was irradiated with one or two monoenergetic electron flood guns in a vacuum chamber at a pressure of 10^{-7} Torr. To avoid undue damage to the sample by arc discharges, the incident electron energy was kept below 6 keV. Both the surface potential and the bulk leakage current were monitored continuously. The samples used in the actual measurements were made from 5 mil aluminized Kapton obtained from the same batch used for making the SSPM flight samples. The samples were assem-

bled by the Air Force Material Laboratory and the aluminized Kapton film was supplied by Sheldahl, Northfield, Minnesota.

RESULTS AND DISCUSSION

Charging under Monoenergetic Irradiation

In this set of experiments, the surface potential of Kapton was monitored while being irradiated with a single electron beam at normal incidence. The energy of the primary beam was varied from several hundred volts to several kilovolts. The results show that the equilibrium surface potential of a low conductivity material, such as Kapton, is clearly dominated by secondary emission. A plot of the measured surface voltage as a function of the primary beam energy is given in figure 2. For beam energies below E_{II}, where $\delta > 1$ (shown in the upper trace), the surface tends to charge up positively instead of negatively. Within this $\delta > 1$ range, the equilibrium surface potential is insensititive to the incident beam energy; a large change in the primary electron beam energy causes only a small change in the surface voltage. However, for incident beam energies near E_{II}, the surface potential drops rapidly as it crosses the zero line. Beyond this point, the surface charges up negatively and the measured potential is directly proportional to the primary beam voltage with a slope of unity. This behavior can be understood by the following explanation.

At low incident beam energy, the kinetic energy of the electron arriving at the surface causes more secondary electrons to be emitted per primary electron, $\delta > 1$. The surface experiences a net depletion of electrons, giving rise to a positive surface voltage. In principle, the magnitude of the positive potential will continue to increase and accelerate the primaries towards the surface until the kinetic energy of the primaries striking the surface is equal to E_{II} where $\delta = 1$. However, the surface is prevented from becoming too positive due to the abundance of low energy electrons around. The reattraction of these low energy electrons pins the surface voltage low and makes it rather insensitive to changes in the incident beam energy. When the beam energy is equal to E_{II}, the number of incoming primaries is exactly balanced by the number of outgoing secondaries. There is no net gain or loss of electrons at the surface and thus the surface becomes uncharged. In figure 2, this corresponds to the point at which the measured surface voltage goes to zero. At this point, E_{II}, the second crossover energy, can be measured directly from the beam voltage. Beyond this point, the beam energy moves into a region where $\delta < 1$. There will be a net absorption of electrons at the surface. The accumulation of these incoming electrons gives rise to a negative potential at surface. This negative potential slows down the incoming primaries and causes δ to increase towards unity. At equilibrium, the surface will charge to a potential such that the electrons arriving at surface will have a kinetic energy equal to E_{II} and a $\delta = 1$. As a result, the surface charges up to a potential equal to beam energy minus E_{II}. Experimental observation agrees quite well with this analysis. At beam energy higher than E_{II}, the surface potential tracks the beam energy linearly and

$$-eV_S = E_B - E_{II} \tag{3}$$

where V_S and E_B are the surface potential and the beam energy, respectively. In addition, the linear relationship between V_S and E_B extends over several kilovolts. This result points out the fact that the secondary emission yield is not sensitive to the surface potential acquired on the material. This is important because the bulk of the secondary emission data reported in the literature were obtained by conventional methods which required the material surface to be at or near ground potential. This finding removes some of the uncertainty concerning the validity of using the data obtained by the conventional methods and applying them to situations where the material is charged to several kilovolts.

Two-Electron Beam Charging

In this section, the charging behavior of a dielectric in a multienergetic electron environment will be discussed. The discussion will be based on the results of a set of charging experiments using two electron guns at different energies. The angle of incidence for each gun was offset about 3 degrees from the sample normal. Based on the data presented in the next section, the effects of this minor offset are negligible and will be ignored in the following discussion.

The significance of secondary emission in a distributed environment can be understood by the following analysis. First consider an insulator being irradiated by a single electron beam. As a result, the surface potential developed is controlled by the energy of the beam, E_{B1}, via secondary emission. As we have shown in the previous section, for beam energy greater than E_{II} of the material, the surface charges up negatively, and, at equilibrium, $-eV_S = E_{B1} - E_{II}$. When the second beam is turned on, the surface potential created by the first beam retards the electrons in the second beam. At the same time, the origin of the secondary electron yield curve is also shifted from zero for an uncharged surface to $-eV_S$ when the surface is charged, as shown on an absolute energy scale in figure 3. In this representation, it is clear that the electrons from the second beam fall into three distinct categories, namely noninteracting, discharging, and charging, depending on the beam energy.

Based purely on an energy argument, electrons with energy lower than the surface potential will be reflected and will not interact with the surface at all. As we increase the energy of the second beam, it is equivalent to moving the arrow for E_{B2} in figure 3 to the right. We note that there is a region between $-eV_S$ and $-eV_S + E_I$ (the first crossover) where the electrons are weakly charging. However, since this region is narrow (~50 V for Kapton) and the effect small, we can safely ignore its contribution. Therefore, electrons from the second beam with energy less than $-eV_S + E_I$ can be considered noninteracting.

In the second category, at higher beam energies, the electrons with E_{B2} between $-eV_S + E_I$ and $-eV_S + E_{II}$ will have the appropriate kinetic energy to impact the surface with a secondary yield greater than one. The net increase in the secondary emission due to the second beam causes the surface to discharge. Consequently, the surface voltage will shift to a lower value V_S' in order to re-establish current balance. At equilibrium, the number of

electrons emitted due to the second beam has to be balanced by the number of electrons absorbed from the first beam, or,

$$\delta(E_{B2} + eV_{S'})J_{B2} + \delta(E_{B1} + eV_{S'})J_{B1} = J_{B2} + J_{B1} \tag{4}$$

where J_{B1} and J_{B2} are the current densities of the first and the second beam at the surface, respectively. The relation described in equation (4) provides a way of sweeping out the shape of the secondary emission yield curve by varying the current densities and the beam energies. However, this way of determining δ is tedious experimentally and requires a great deal of curve fitting and optimization. Fortunately, a faster and more convenient method has been developed for determining the secondary emission yield curve by measuring E_{max} and E_{II} for a particular material.

In this method, the dielectric is irradiated simultaneously with two electron beams. The energy of one beam is fixed while a second, the probe beam, whose intensity is modulated scans continuously over a wide range of energy. The current of the probe beam is deliberately kept low in order not to disturb the equilibrium surface voltage established by the first beam. In this measurement, the surface voltage is monitored continuously and the small AC component in surface voltage induced by the modulated probe beam is measured by synchronous detection. The amplitude and phase of the AC component are determined by the number of electrons emitted or absorbed by the surface due to the probe beam. Hence, a plot of the synchronous change in surface voltage as a function of the energy of the probe beam is directly related to the secondary emission yield curve of the material. Such a plot and the experimental conditions used are shown in figure 4 from which we can extract E_{max} and E_{II} directly. For Kapton, we found that E_{max} = 250 V and E_{II} = 1000 V. These values agree with those determined previously in our laboratory. Figure 5 shows the secondary yield curve for Kapton obtained from equation (2) using the values given above. These results show that the modulated probe beam method offers a convenient and accurate way for determining the secondary emission properties of various film-type dielectric materials.

Once the shape of the secondary emission curve is determined, the charging response of a material to a multienergetic electron flux, F(E), can be understood. As discussed earlier, the spectrum of these electrons can be divided into three critical regions, as shown in figure 6. Electrons with energy below $-eV_S + E_I$ are noninteracting and can be eliminated right away. Between $-eV_S + E_I$ and $-eV_S + E_{II}$, electrons have a $\delta > 1$ and a tendency to discharge the surface. Above $-eV_S + E_{II}$, because $\delta < 1$, electrons in this region tend to cause the surface to charge negatively. In order to maintain current balance for a material with zero leakage, the total number of electrons emitted ($\delta > 1$) must be balanced the electrons absorbed ($\delta < 1$). Hence,

$$\int_{-eV_S}^{E_u} \left[\delta(E + eV_S) - 1\right] F(E)dE = 0 \tag{5}$$

where E_u is the highest energy of the nonpenetrating electrons and F(E) is the incident electron flux at normal incidence. When equation (5) is not

satisfied, V_S will shift to a new surface potential V_S' until current balance is reestablished. Similarly, a change in the electron distribution will result in a change in the surface voltage. Therefore, conceptually, this analysis provides a physical link between the properties of the material and the electron distribution of the environment in determining its surface potential. It should be noted that, in the absence of photoillumination (causing photoemission and photoconductivity), secondary emission is the most important factor in controlling surface charging of low-conductivity materials. However, a number of other effects, such as electron induced conductivity and ion induced secondary emissions, have to be considered in the order to make the analysis more applicable to actual substorm charging in space.

Angular Dependence

In the preceding discussion, it has been assumed that the primary electrons strike the material surface at normal incidence. However, it is well known that oblique incidence produces more secondaries than normal incidence. This is due to the fact that the secondary electrons are generated closer to the surface and have a greater probability of escaping from the solid. As a result, both E_{max} and E_{II} in equation (2) will increase as the angle of incidence increases. Hence, the dependence of these parameters on incident beam angle is critical to understanding the charging behavior of materials in space where the incident electrons may strike from all directions.

Recent analyses indicate that the electron angular distributions in near geosynchronous orbits are highly anisotropic during geomagnetically disturbed times. An estimate indicates that the electron current normal to the earth's magnetic field line is roughly three times larger than the current parallel to the field line (fig. 7). The data presented in the figure were obtained from a natural charging event on Satellite P78-2 on February 12, 1979. The angular distribution of the electron current was obtained by integrating the electron flux between 3.4 and 19.4 keV provided by the SC-2 particle counter on board P78-2. In figure 7, the angularly resolved current was plotted as a function of magnetic angle and universal time (UT) in seconds for three consecutive satellite spin cycles. Each spin cycle is about 60 seconds long. Due to symmetry along the magnetic axis, the current-angle profile is approximately the same in each half cycle. Since this charging event was occurring in the sun and the direction of the solar radiation was approximately parallel to that of the current maximum, charging of the SSPM samples could only take place in the dark half cycle of each satellite rotation. Since the SC-2 particle counter and the SSPM are located at different parts on the spacecraft, there is a time delay between the two measurements. The crosses in figure 7 mark the onsets of the dark half cycles from which the SSPM charging data presented in figure 8 were obtained. The solid lines in figure 7 represent, given the time delay, approximately the current profiles that would impinge on the SSPM in the dark half cycles marked by the crosses respectively. Notice in figure 8 that, during the first dark half cycle (UT = 18292), the Kapton surface did not show any sign of charging until the sample rotated to within 30 degrees [120°] from the current maximum [90°]. The angles quoted in brackets are the magnetic angles given in figure 8. In the next dark half cycle (UT = 18346), the electron distribution in the plasma sheet hardened and the peak current in figure 7 went up. During this time, the Kapton sample began to charge earlier

(about 55 degrees [145°] from the maximum) and subsequently charged to a higher potential. In the last half cycle, the electron distribution softened slightly and the Kapton charging profile is intermediate between the profiles in the first and second half dark half cycles, it did not begin to charge immediately. Instead, charging occurred only when the angle of incidence of the peak current approached normal incidence. In addition, the onset and the magnitude of charging are highly correlated to the intensity of the peak current. These results show that charging is quite sensitive to the anisotropy of the electrons in the plasma sheet. Hence, there is a need to understand how the angle of incidence influences the charging behavior of dielectrics.

In the laboratory, a monoenergetic charging beam was used to examine the effects of varying the angle of incidence on charging. The equilibrium surface voltage was found to decrease with increasing angle of incidence as expected from higher secondary emission. Figure 9 shows a family of charging curves for Kapton at different angles of incidence. When the threshold beam voltages for surface charging and the slopes of the charging curves of figure 9 are plotted against the angle of incidence, θ, they are found to follow $\cos^2\theta$ (fig. 10). From these results, we found that the angular dependence of the equilibrium surface potential is given by

$$-eV_S(\theta) = \cos^2\theta\, E_B - E_{II}^o \tag{6}$$

where E_{II}^o is the second crossover energy of the material at normal incidence and E_B the primary electron energy. Consequently, the angular dependence of the second crossover, $E_{II}(\theta)$, for Kapton can be determined by setting $-eV_S(\theta) = 0$, and, $E_{II}(\theta) = E_B$,

$$E_{II}(\theta) = \frac{E_{II}^o}{\cos^2\theta} \tag{7}$$

The same angular dependence can be obtained by applying Sternglass' theory. These results indicate that, for a particular material, the momentum-loss mean free path controls the production of the secondaries and hence the charging characteristics of the material. They further suggest that the secondary emission yield should increase as $(\cos^2\theta)^{-1}$ with increasing angle of incidence. However, more work is needed to confirm the validity of this dependence.

SUMMARY

In the absence of light and high energy particles, the surface potential of Kapton is found to be controlled by secondary emission. Under monoenergetic electron irradiation, the surface voltage varies linearly with the beam voltage. In a multienergetic environment, the surface voltage is determined by the convolution of the electron distribution and the secondary electron yield of the material. Using single and dual electron beam charging techniques, we have devised methods for measuring the critical secondary emission yield parameters as well as the angular dependence of these parameters for Kapton. This information is not only essential to the understanding of mate-

rial charging in space but also valuable as input to the NASCAP spacecraft charging modeling code.

REFERENCES

1. Space Systems and Their Interaction with Earth's Space Environment, edited by H. B. Garrett and C. P. Pike, Progress in Astronautics and Aeronautics, Vol. 71, American Institute of Aeronautics and Astronautics, New York, N.Y.
2. Purvis, C. P.: Status of Material Characterization Studies, Proceedings of Spacecraft Charging Technology Conference, R. C. Finke and C. P. Pike, eds., AFGL-TR-79-0082, NASA Conference Publication 2071, pp. 437-456.
3. Dekker, A. J.: Secondary Electron Emission, Solid State Phys., Vol. 6, 1958, pp. 215-311.
4. Sternglass, E. J.: Secondary Electron Emission and Atomic Shell Structure, Phys. Rev., Vol. 80, 1950, p. 925.
5. Stevens, J. R.: Description of Space Test Program P78-2 Spacecraft and Payloads, SAMSO TR-78-4, 1978.

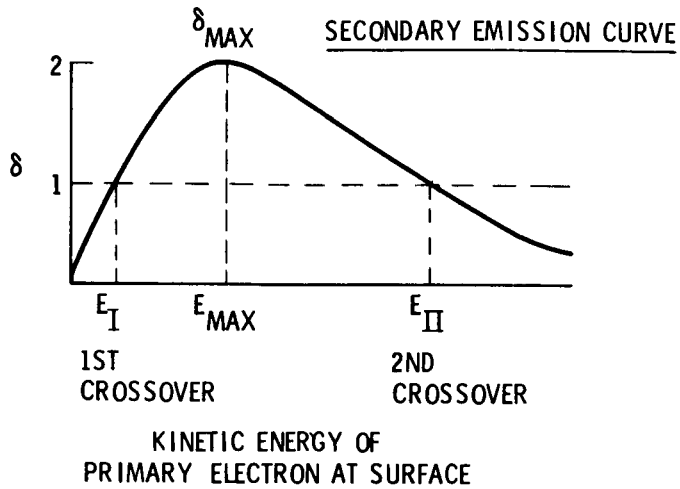

Figure 1. - A "typical" secondary emission yield curve of an insulator.

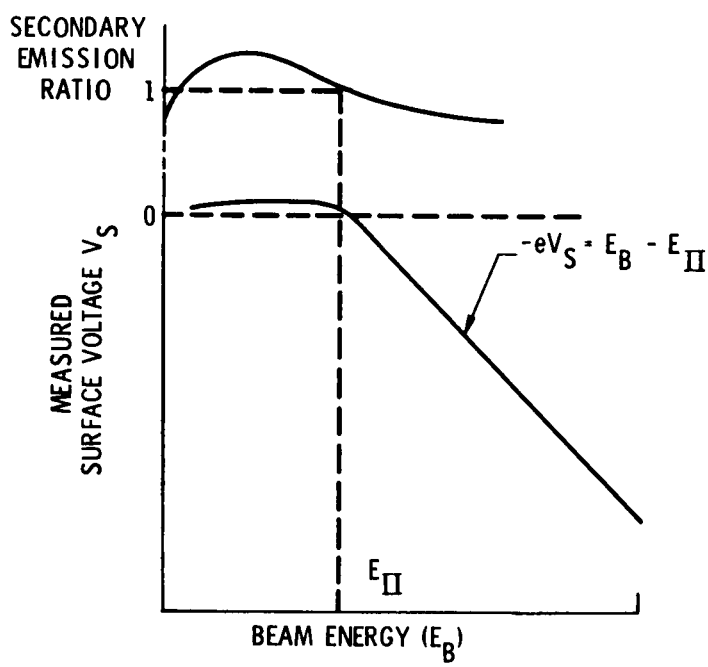

Figure 2. - Charging behavior of a low-conductivity material under monoenergetic electron irradiation. The top trace is the secondary emission yield curve and the bottom trace is the measured surface voltage vs beam energy.

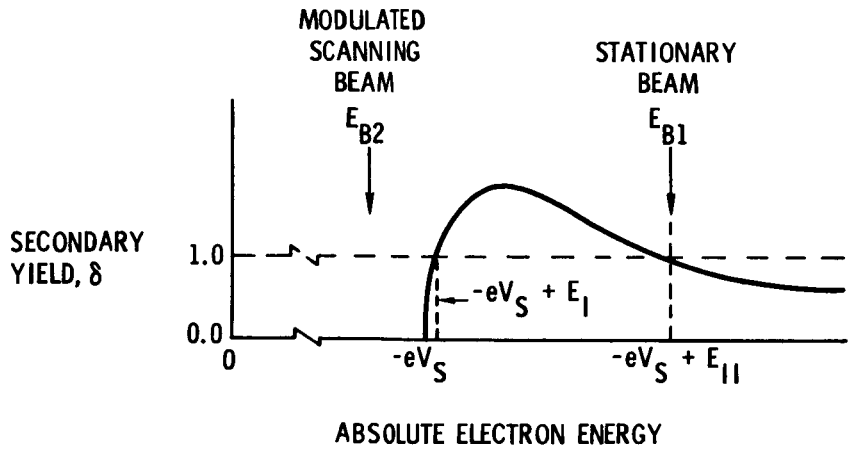

Figure 3. - For a charged surface, the origin of the secondary electron yield curve is shifted to $-eV_S$ on an absolute energy scale. The arrows indicate the energies of the stationary and scanning electron beams.

BEAM	ENERGY (eV)	DENSITY ($1/cm^2$)
No. 1 (stationary)	4000	1.0 nA
No. 2 (scanning)	2500-5000	10 pA (100% AM)

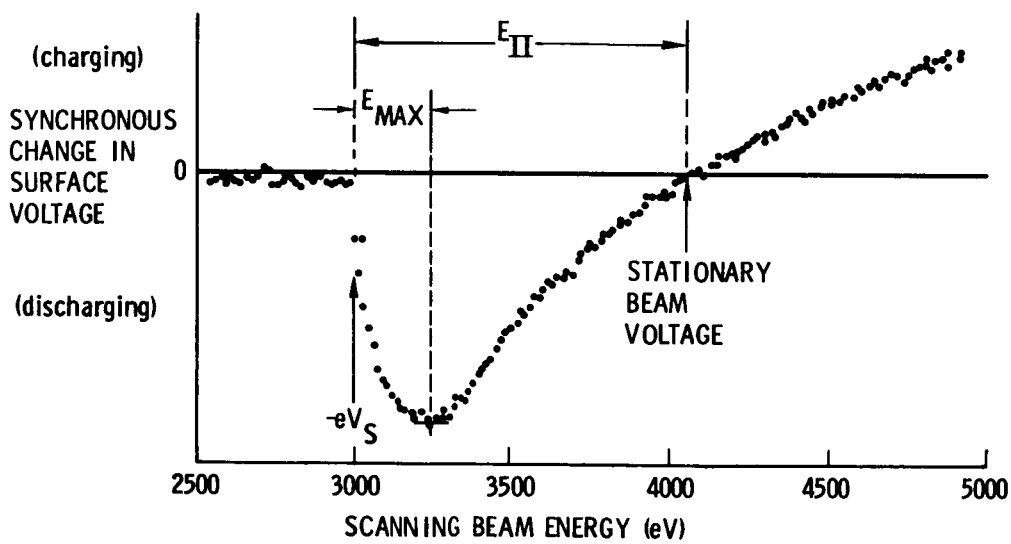

Figure 4. - Results of the modulated two-beam charging experiment. E_{max} and E_{II} can be obtained directly from this plot.

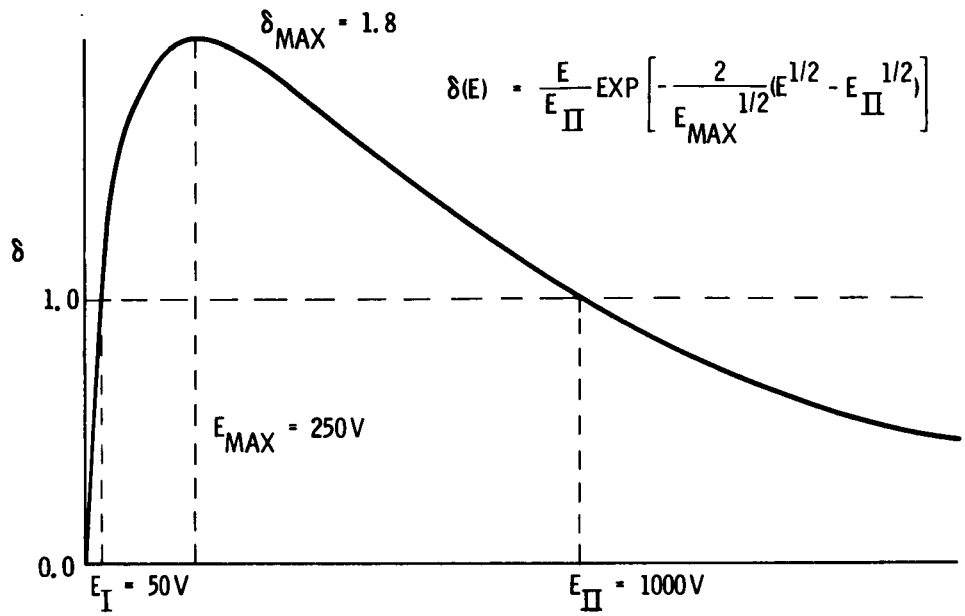

Figure 5. - Secondary yield curve for Kapton obtained from equation (2) by using the values determined by the modulated beam method.

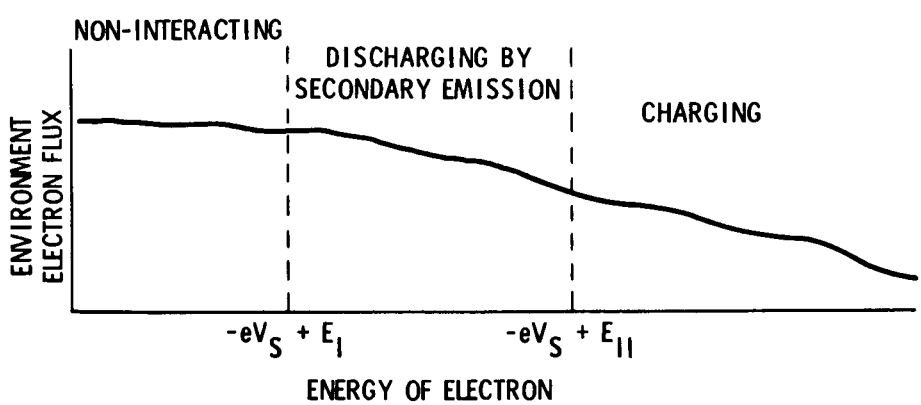

Figure 6. - Electron distribution separated into three distinct regions: noninteracting, discharging ($\delta > 1$), and charging ($\delta < 1$).

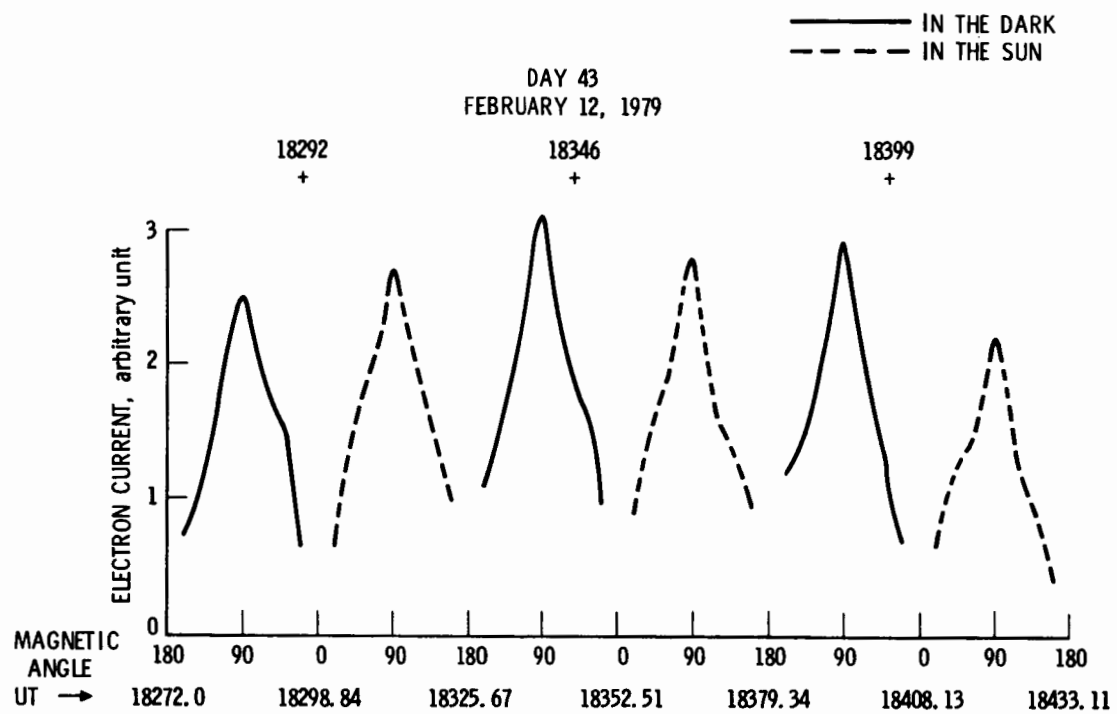

Figure 7. - Anisotropy in electron angular distribution during a "typical" charging event. Current-angle profiles are shown for three consecutive satellite rotations.

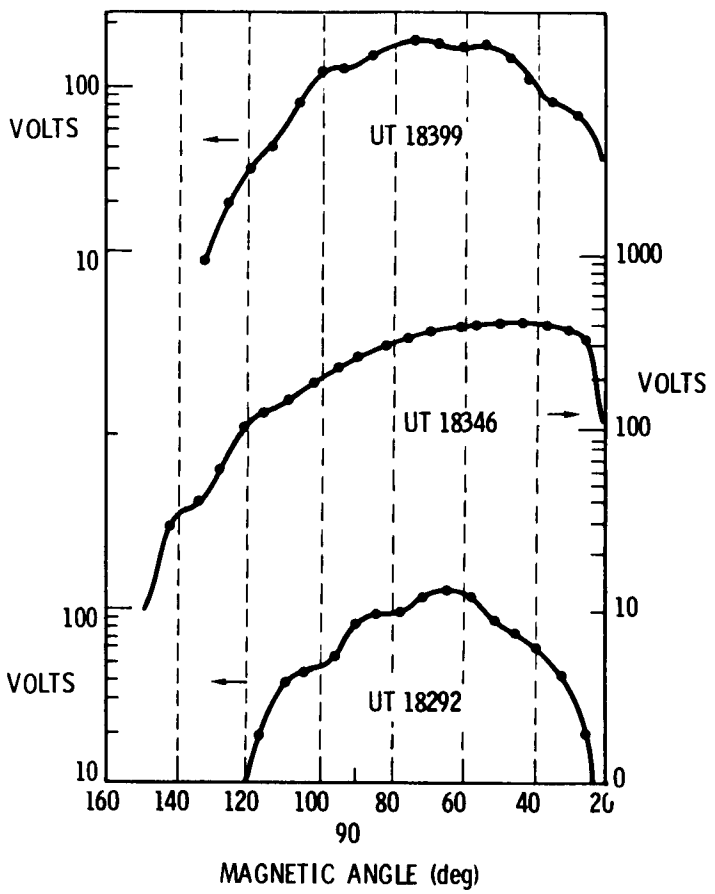

Figure 8. - Charging response of SSPM Kapton to the anisotropic electron environment described in figure 7.

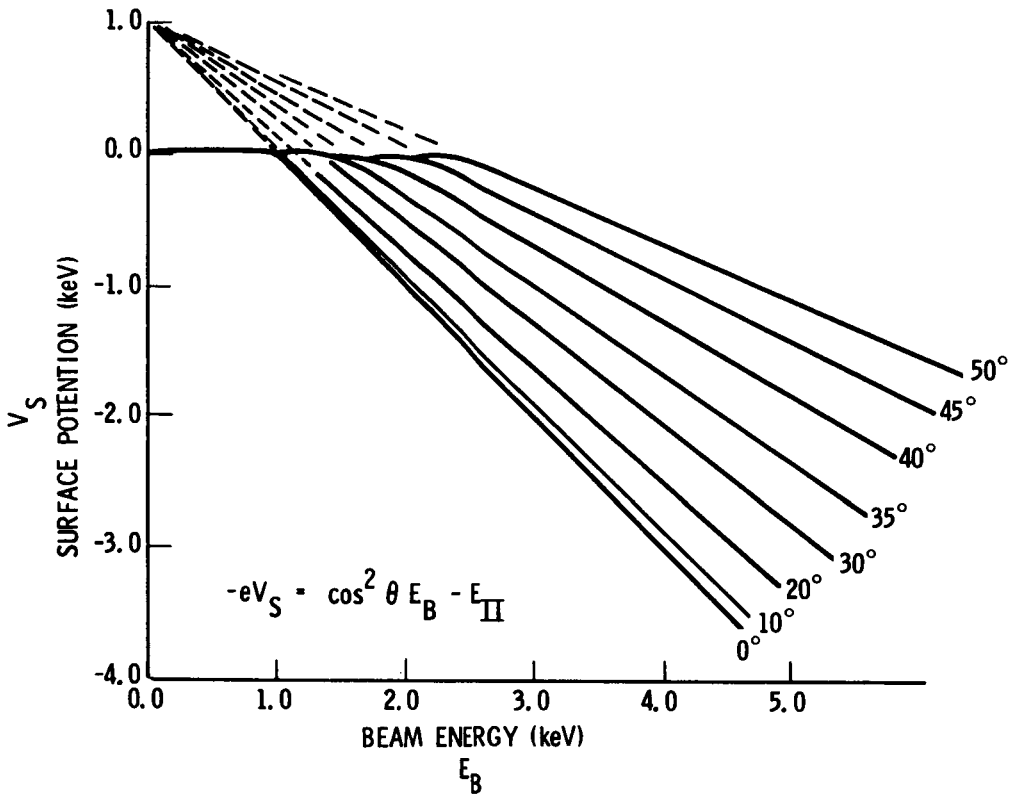

Figure 9. - Monoenergetic charging curves of Kapton at different angles of incidence.

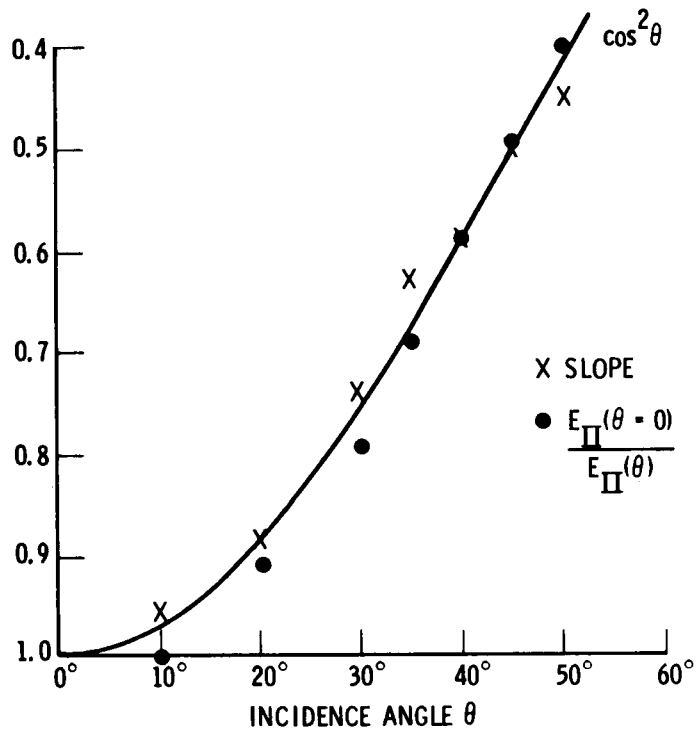

Figure 10. - Variation of threshold beam voltage and charging slope as a function of angle of incidence.